Carbonsphere, **2026, 2, 9510007**

Research Article

Climate change increases aqueous ecological risks of semi-volatile organic compounds: a meta-analysis and mechanistic modeling in three major watersheds

Tingting Sun[1], Mingliang Fang[2,*], Jingyu Zhu[3], Lusha Zeng[1], Fanrong Zhao[4], Changzhi Shi[2], Shuhan Ren[1], Ke Yin[1,*], Qianhong She[3], Xunchang Fei[3,5,*]

1 Department of Environmental Engineering, College of Ecology and Environment, Nanjing Forestry University, Nanjing 210037, China

2 Department of Environmental Science and Engineering, Fudan University, Shanghai 200433, China

3 School of Civil and Environmental Engineering, Nanyang Technological University, Singapore 639798, Singapore

4 Department of Applied Chemistry, China Agricultural University, Beijing 100193, China

5 Nanyang Environment and Water Research Institute, Singapore 637141, Singapore

Address correspondence to Mingliang Fang, mlfang@fudan.edu.cn; Ke Yin, yinke@njfu.edu.cn; Xunchang Fei, xcfei@ntu.edu.sg

Received: November 25, 2025 / Revised: January 17, 2026 / Accepted: April 16, 2026

Abstract

Semi-volatile organic compounds (SVOCs), represented particularly by polycyclic aromatic hydrocarbons (PAHs), are notorious pollutants that significantly affect aquatic ecosystems and public health. Sediments serve as major sinks for anthropogenic PAHs, yet their role in modulating aquatic ecological risks of PAHs under climate change scenarios remains underexplored. We combined a global meta-analysis of PAHs concentrations in air, water, and sediment from 1993 to 2021 with a robust multimedia fugacity model to assess the transport and distribution of PAHs. The toxicity equivalent concentration approach is used to calculate the Risk Quotient and Dioxin Toxicity Equivalence of PAHs. We found that the majority of the reported measurements clustered in three major watersheds: Yangtze (n = 488) and Huanghe (n = 196) in China, and St. Lawrence (n = 337) in the United States. We reveal that sediment sinks contribute substantially to the persistence and redistribution of PAHs. By 2050, high molecular weight PAHs will dominate the sediment–water exchange pathway, while low molecular weight PAHs will be largely depleted in sediments, primarily driven by projected shifts in emission composition, enhanced volatilization and degradation of low molecular weight compounds, and the absence of continuous external inputs. Climate-induced changes in sediment fluxes are predicted to elevate the aquatic PAHs concentrations and associated risks, quantified by Risk Quotient and Dioxin Toxicity Equivalence, in China. While this trend holds for most regions, the St. Lawrence watershed is projected to see lower ecological risk due to higher PAHs degradation rates. This research underscores the critical role of sediment sinks in shaping PAHs risks under climate change and emphasizes the need for integrated management strategies, including sediment remediation and climate change adaptation.

Keywords: PAHs, sediment sinks, climate change, aquatic ecological risk

1. Introduction

Polycyclic aromatic hydrocarbons (PAHs) are ubiquitous and highly toxic semi-volatile organic compounds (SVOCs) that pose serious risks to aquatic ecosystems and human health [1, 2]. Exposure to PAHs, which can occur through inhalation, ingestion, or dermal contact, is linked to various adverse health outcomes, including carcinogenicity, respiratory issues, and developmental toxicity. Despite global reductions in PAHs emissions—which peaked at 592 Gg in 1995 and are projected to decrease by 46-71% between 2009 and 2030 [3], PAHs inputs to lake sediment between 2002 and 2018 have increased [4], and PAHs concentrations in the coastal water of ports worldwide exhibit incremental trends [5, 6]. Meanwhile, the studies of temporal trends in PAHs concentrations in sediment since 2000 unveil relatively stable concentrations globally [5]. These findings suggest a disproportionate redistribution among gas, aqueous, and solid phases driven by biogeochemical cycles and ongoing exchanges.

Sediments act as significant sinks for PAHs, trapping these toxic compounds while also serving as a source under certain environmental conditions. Sediment-bound PAHs are subject to dynamic processes like deposition, diffusion, and resuspension, which are further influenced by climate change. Rising temperatures altered precipitation patterns, and more frequent extreme weather events exacerbate the remobilization of sediment-bound PAHs, amplifying their ecotoxicological impacts in aquatic systems. In contrast, low molecular weight (LMW) PAHs, typically comprising 2–3 aromatic rings, exhibit higher volatility and water solubility. These properties facilitate their rapid exchange between air and water phases, leading to greater potential for atmospheric transport and volatilization from aquatic systems. Although LMW PAHs are generally less persistent and toxic than their HMW counterparts, they can still contribute to acute ecological stress. High molecular weight (HMW) PAHs demonstrate strong hydrophobicity and persistence, making them dominant contributors to ecological and health risks.

Watersheds, with their complex networks of interconnected water bodies, play a critical role in mediating PAHs transport across air, water, sediment, and soil (Fig. S1, Supplementary

Information (SI)). PAHs enter watersheds through dry and wet deposition (F_D) [7-9] and air-water exchange (F_{AW}) [10-13]; while within a watershed, PAHs migrate between sediment and water via diffusion (F_{SW}) [14-17], facilitated by groundwater discharge, sediment resuspension, and biotic activity [18]. Recent studies suggest that bubble ebullition also contributes to PAHs transport (F_{GE}) from sediment to water [19-21]. PAHs can be diluted by precipitation and biodegradation [22] (Fig. S1, SI). F_D and F_{GE} are one-way processes transporting PAHs to the water, whereas F_{AW} and F_{SW} are reversable (Fig. S1, SI). Climate-induced alterations in temperature, humidity, and precipitation patterns further complicate these interactions, potentially increasing volatilization of LMW PAHs and deposition of HMW PAHs.

The time-dependent evolutions of PAHs concentrations across these phases in influenced by multiple factors [23], including dynamic PAHs emissions, characteristics of PAHs sinks, and transport pathways. For instance, the emissions of PAHs congeners depend on factors such as fuel type, season, combustion efficiency [24, 25], heating demands [26], photo- and thermo-chemical oxidations [27-29], and meteorological conditions [30, 31]. Aqueous PAHs concentrations are influenced by biogeochemical cycles, atmospheric deposition, natural water flow, and sediment discharge [32-34], while PAHs concentrations in sediment and soil are primarily governed by the partition coefficients of individual PAHs between soil organic matter (SOM) and water (K_{oc} values) [35]. As climate change alters precipitation patterns and intensifiers storm events, these processes may be further complicated, leading to unpredictable PAHs behavior in watersheds. Climate change is poised to exacerbate the complexities of PAHs behavior. Alterations in temperature, humidity, and precipitation patterns can influence PAHs volatilization, deposition, and degradation, potentially leading to greater volatilization of LMW PAHs and increased deposition of HMW PAHs in certain regions. These climatic shifts could amplify the risks associated with PAHs contamination, particularly in vulnerable watersheds.

Past studies often focused on short-term temporal trends within isolated small systems, e.g., monitoring a single lake system for weeks or months [23], and employing two or three-phase models

to predict PAHs concentrations in terrestrial water [36] while ignoring climate impacts. A more sophisticated approach, such as meta-analysis combined with climate change and mechanistic modelling [37], e.g., a multimedia fugacity framework, which incorporates a whole set of attributes from a typical watershed, is essential for predicting the behavior of PAHs in different environmental compartments [38]. To this end, overall trends [39] and key factors driving regional PAHs concentrations in the context of a changing climate [40] is enlightened. However, most large-scale PAHs measurements and modeling trials concentrated on oceanic systems [1, 8, 22, 41, 42], with terrestrial studies being extremely limited due to a lack of time- and location-dependent PAHs concentration big data [32, 43].

In this study, we aim to predict individual concentrations and aggregative aquatic toxicity of 16 PAHs congeners in major watersheds under the dual influences of global energy market shifts and climate change, with a focus on achieving sustainable management of water aligned with Sustainable Development Goals (SDG) target 6.3. We conducted a comprehensive meta-analysis of global PAHs measurements, including spatiotemporal profiles of congener-specific concentrations and degradation factors. We then established a robust non-steady-state open system multimedia fugacity model (OSMF) to predict PAHs concentrations in the air, surface water, and sediment of three representative watersheds with extensive available monitoring data: the Huanghe, Yangtze, and St. Lawrence. This research pioneers in quantifying global PAHs distribution, transport, and aqueous ecotoxicity in the context of climate change, providing crucial insights for policymakers to formulate effective, region-specific prevention and remediation strategies.

2. Methods

2.1. Literature review and data collection

Between September 2020 and December 2024, we collected data on 16 USEPA-prioritized PAHs from Web of Science and Google Scholar, focusing on studies from 1990-2020 (Fig. S2, SI). The dataset includes 931 water samples, 290 air samples, and 1521 sediment samples across Asia,

Europe, and North America (Table S1-3S, SI). Samples were grouped into 5-year intervals to analyze temporal trends. Due to the limited data, South America and Africa were excluded. The study compares PAHs concentrations across East Asia (primarily Chinese waters), Europe (primarily Western Europe waters) and the North America Great Lakes.

2.2.Non-steady-state OSMF model for PAHs transport and degradation

PAHs are categorized into low molecular weight (LMW, 2-3 rings), including naphthalene (NAP), acenaphthylene (ACY), acenaphthene (ACE), fluorene (FLU), phenanthrene (PHE), and anthracene (ANT), and high molecular weight (HMW, 4-6 rings) categories, including fluoranthene (FLA), pyrene (PYR), benz[a]anthracene (BaA), chrysene (CHR), benzo[b]fluoranthene (BbF), benzo[k]fluoranthene (BkF), benzo[a]pyrene (BaP), indeno[1,2,3-cd]pyrene (IcdP), dibenz[a,h]anthracene (DahA) and benzo[g,h,i]perylene (BghiP). Transport pathways — air-water exchange, atmospheric deposition (Table S4, SI), sediment-water diffusion, and bubble ebullition, were analyzed for three major watersheds (Yangtze, Huanghe, and St. Lawrence). We derived 5-95% percentiles of PAHs concentrations in the air, water, and sediment and orthogonalized these factors (Fig. S3-S4, SI). We further evaluated PAHs migration in the water phase under the non-steady-state OSMF framework combined air-water exchange equilibrium and sediment-water diffusion equilibrium. The study made the following assumptions: (1) changes in PAHs concentrations in EA, EU and NA surface waters are determined by net fluxes of F_D, F_{AW}, F_{GE} and F_{SW} coupled with degradation; (2) regional atmospheric PAHs concentrations are proportional to PAHs emissions; (3) point (e.g., manufacturers) or non-point source (e.g., surface runoff) input of PAHs to the surface water and sedimentation are neglected; (4) potential PAHs degradation in the surface water is determined from regression analysis on historical data (Table S5, SI). It is also important to note that the OSMF framework is not as a high-precision regional prediction model given that point source PAHs inputs were not included in our predictions; future models should account for these inputs to enhance accuracy. The three watersheds were

classified into four temperature zones based on latitudes (< 22.4°, 22.4-54°, 54-66°, > 66°), with temperature-dependent parameters adjusted accordingly (Fig. S5-S6 and Table S6, SI).

2.3. Air-water exchange flux

PAHs exchange between air and water (F_{AW}, ng/m^2/d) was modeled using Fick's law of two–film theory [44] incorporating Henry's law and meteorological factors,

$$F_{AW} = K_{AW} \times (1000 \times C_w - \frac{C_A}{H'}) \text{ eq (1)}$$

Where C_a and C_w are the average concentrations of air (ng/m^3) phase and dissolved PAHs in water phase (ng/L) respectively, K_{aw} is the air-water mass transfer coefficient (m/d) calculated using the two-film model [45], and H' is the dimensionless Henry's constant. The dimensionless Henry's law constant (H') is calculated from equation (2) [46, 47],

$$H' = H \div (R \times T) \text{ eq (2)}$$

Here, H is the temperature- and salinity-corrected Henry's law constant (Pa/m^3/mol), R is universal gas constant (8.314 Pa m^3/kmol), and T(k) is the absolute temperature of the air-water interface. The air-water mass transfer coefficient (K_{aw}) comprising resistances to mass transfer across the air (K_a, m/d) and water (K_w, m/d) is calculated as [48]:

$$1/K_{aw} = 1/K_w + 1/(H'K_a) \text{ eq (3)}$$

$$K_a = 10^{-3} + 4.62 \times 10^{-2} \times U^* \times S_c \times (a)^{-0.67} \text{ eq (4)}$$

$$K_w = 10^{-6} + 34.1 \times 10^{-4} \times U^* \times S_c \times (w)^{-0.5} \ (U^* > 0.3\ m/s) \text{ eq (5)}$$

$$K_w = 10^{-6} + 1.44 \times 10^{-2} \times (U^*)^{2.2} \times S_c \times (w)^{-0.5} \ (U^* < 0.3\ m/s) \text{ eq (6)}$$

$$U^* = 10^{-2} \times (6.1 + 0.63 \times U_{10})^{0.5} \times U_{10} \text{ eq (7)}$$

$$S_c(w) = 5.42 \times MW + 825.04 \text{ eq (8)}$$

$$S_c(a) = 0.0033 \times MW + 1.85 \text{ eq (9)}$$

where U* is the flow velocity of PAHs in the air (m/s); U_{10} is the wind speed at a height of 10 m above the water surface (m/s)[49]. S_c(w) and S_c(a) are the Schmidt values of PAHs in the water and air, respectively; MW is the molecular weight of the PAHs. According to the literature, the wind

speed (U*) in Asia, Europe, North America, and South America is 0.027 ± 0.007, 0.031 ± 0.010, 0.032 ± 0.009, and 0.032 ± 0.005 m/s, respectively.

2.4. Sediment-water diffusion flux

Sediment-water diffusion followed Fick's gradient flux law, assumed a well-mixed sediment layer. The flux is calculated as follows:

$Fsw = K_s \times (C_{pw} - C_w)$ eq (10)

Where, F_{SW} (ng/m^2/d) is the diffusion flux of PAHs between the sediment and water, C_{pw} and C_w are the concentrations of PAHs in sediment pore water and the upper water column (ng/L), and K_s (m/d) is the sediment-water mass transfer coefficient. Ks can be calculated by the following formula:

$K_s = D_w \div h$ eq (11)

Where, D_w (m^2/d) is the molecular diffusion coefficient of PAHs, which is temperature-dependent, and h (m) is the thickness of the boundary layer, and the value of h in this paper is set to 0.0012m [50].

PAHs concentrations in sediment pore water are calculated using:

$C_{pw} = C_s \div (K_{oc} \times f_{oc})$ eq (12)

Where, C_s is the PAHs concentration in dry sediment (ng/g d.w.); K_{oc} is the organic carbon-water partition coefficient (Table S6, SI); and f_{oc} is the organic carbon content (wt.%).

2.5. Bubble-ebullition facilitated flux

Bubble transport was estimated based on gas-phase partitioning and interface adsorption models [19] (Table S7, SI). The PAHs flux due to gas phase partitioning is estimated using Henry's law [20, 51],

$F_{GE,PAH1} = 22.4 \times H' \times C_{pw} \times GF_{Ebull} \div V_{CH_4}$ eq (13)

Where 22.4 is the molar volume of a gas at standard temperature and pressure (STP, 32° Fahrenheit and 1 atm, L/mol); $F_{GE,PAH1}$ is the PAHs flux facilitated by bubble portioning (mg/m^2/d); GF_{Ebull} is

the bubble ebullition flux (mmol CH_4 m^2/d); V_{CH4} is the percentage volume (vol.%) of gas in the bubbles (set at 60%).

The flux due to bubble surface adsorption is calculated as [52],

$F_{GE,PAH2} = 6 \times K_{ia} \times F_{GE,PAH1} \div d$ eq (14)

$K_{ia} = K_{iw} \div K_{aw}$ eq (15)

Where $F_{GE,\ PAH2}$ is the PAHs flux facilitated by bubble interface adsorption (mg/m^2/d); K_{ia} (m^3/m^2) is interface-air partitioning coefficient, which is defined as the ratio between interface-water partitioning coefficient (K_{iw}) to air-water (Table S6, SI) partitioning (K_{aw}); d is the average bubble diameter (m); while the number 6 is the coefficient of volume calculation residue ($V = \pi \times d^3 \div 6$). (Note, the air-ocean exchange is benchmarked as a background value of the F_{AW} for PAHs, with the net F_{AW} in the Atlantic Ocean, Pacific Ocean, and Indian Ocean being (0.8-1.4) $\times 10^4$ ng/m^2/d, (1.4-2.6) $\times 10^4$ ng/m^2/d and (0.4-0.7) $\times 10^4$ ng/m^2/d, respectively (Fig. S7, SI)).

2.6. Predictions of regional PAHs emissions and water concentrations

Historical PAHs emissions (1999-2014) [3] were analyzed as functions of energy consumptions and gross domestic production (GDP):

$F_{PAHi} = a \times E_i^{r_1} \times GDP_i^{r_2}$ eq (16)

Where F_{PAHi} stands for the total PAHs emissions of region i. Ei stands for energy consumptions of region i. GDPi stands for GDP of region i. r_1 and r_2 are constant elasticities between PAHs and energy or GDP in the function.

The change of PAHs concentration in water phase and the change trend of the water-air exchange flux that changes dynamically with the change of air phase and water phase concentration are predicted according to the four processes of water-air exchange, dry and wet deposition, sediment-water diffusion, and bubble ebullition.

$F_{AW,i} = K_{aw} \times (1000 \times C_{w,i} - C_{a,i} \times R \times T \div H)$ eq (17)

$C_{a,i} = C_{a,2020} \times E_{a,i}$ eq (18)

$$F_{D,i} = F_{D,2020} \times E_{a,i} \text{ eq (19)}$$

$$F_{SW,i} = K_s \times (C_{pw,,i} - C_{w,i}) \text{ eq (20)}$$

$$C_{w,i+1} = \left(Q_{Water,i} - F_{AW,i} + F_{D,i} + F_{GE,i} + F_{SW,i}\right) \times \overline{DF} \div V_{Water} \text{ eq (21)}$$

Where, $F_{AW,i}$ is the water-air exchange flux occurred in the i-th year, $C_{w,i}$ and $C_{a,i}$ is the concentration of PAHs in the water and air in the i-th year, $C_{a,2020}$ and $F_{D,2020}$ is the concentration in the air and deposition flux of PAHs in 2020, $E_{a,i}$ is the scaling factor calculated according to the PAHs emission in the air, $\overline{DF}$ is the average degradation factor; V_{water} is the volume of surface water, in which, it is assumed that the PAHs flux ($F_{GE,i}$) promoted by bubble ebullition remains unchanged.

We use the arithmetic mean of PAHs concentrations in air, water, and sediment from different continents over the past 10 years as the initial boundary for the baseline scenario, and integrated projected atmospheric PAHs emissions (by a 1-year operator) to derive future aqueous PAHs concentrations with iteration (by a 1-month operator). The model was validated against historical surface water PAHs concentrations (Fig. S15, SI). C_w in EU was largely consistent with the past regional average PAHs emission profiles. Although the correlation in EA and NA regions was rather moderate, both showed statistical significance (R^2 = 0.24 (EA), 0.83 (EU), and 0.51 (NA), $p < 0.05$, Table S8, SI), reflecting broad-scale trend consistency.

2.7. Risk assessments of aqueous PAHs

The risks of aqueous PAHs are commonly characterized by assessment indices such as Risk Quotient (RQ) and Toxic Equivalent Quantity (TEQ).[53] RQ is the most commonly used ecological risk assessment index for water [54]. RQ < 1, 1 < RQ < 100, and RQ > 100 indicate that PAHs pose no particular risk, moderate and potential risk, and high ecological risk, respectively [54]. The RQ does not respond proportionally to changes in $\Sigma 16C_w$, given the different ecological hazards of individual congeners.

Aqueous PAHs risk was quantified using risk quotients (RQ) (Eq. 22):

$RQ = PEC \div PNEC$ eq (22)

Where PEC is the predicted environmental concentration (equal to C_w), and PNEC is the predicted no effect concentration for three different aquatic organisms – algae, crustaceans and fish, calculated by dividing the LC_{50} or EC_{50} value by an appropriate assessment factor (AF) as follows (eq 23):

$PNEC = LC_{50}\ or\ EC_{50} \div AF$ eq (23)

An AF of 1000 is used in prioritization of PAHs in this study, where short-term toxicity data is adopted in three trophic levels (algae, crustaceans and fish). LC_{50} or EC_{50} values were obtained from literature search or estimated using the Toxicity Estimation Software Tool (TEST, version 5.1) (Table S9, SI).

Carcinogenic risk was evaluated using the TEQ. The toxicity potential of each chemical was represented TEQ, which was estimated by a single PAHs concentration and the Toxic Equivalency Factor (TEF). The total toxicity of the sample was expressed by the sum of the TEQs of the individual PAHs compounds, and the formula was as follows:[55]

$TEQs = \sum TEQ_i = \sum (C_I \times TEF_i)$ eq (24)

Uncertainty was addressed through Monte Carlo simulation (10,000 runs), considering variability in mass transfer coefficients (K_{aw}, H, C_a and C_w) based on their literature-reviewed value range was used. Statistical analyses were carried out in R 3.6.3 and Microsoft Excel. In addition, we assume that PAHs toxicity is additive without interactions may also contribute to uncertainty in risk assessments.

2.8. Uncertainty analysis and model applicability

Uncertainty in the present simulation primarily arises from (1) assumptions regarding PAH sources and dominant transport processes into surface waters, and (2) constrains using literature-derived physicochemical properties and independently reported concentration ranges. While fully independent regional calibration datasets were not available for all regions. As point and non-point

terrestrial runoff sources were not explicitly included, the predicted aqueous PAHs concentrations mainly reflect inputs from atmospheric deposition (dry and wet), air–water exchange, sediment–water diffusion, and bubble ebullition. *Monte Carlo* analysis indicates that atmospheric deposition and sediment–water diffusion contribute most to long-term PAHs mass balance in watershed waters, whereas air–water exchange plays a secondary but non-negligible role, particularly for low molecular weight PAHs.

It is acknowledged that, in highly human-impacted watersheds, riverine runoff and advective renewal can exceed air–water exchange in magnitude. However, the present framework targets long-term, climate-driven responses of the air–water–sediment system, under which sediment acts as a persistent reservoir and regulator of aqueous PAHs. In less disturbed or quasi-reservoir-like watersheds, such as large rivers with extensive floodplains or long water residence times, interfacial exchange processes become increasingly important.

The emission inventory employed in this study represents atmospheric PAHs emissions, which enter surface waters predominantly through dry and wet deposition rather than direct discharge. Consequently, the model is not intended to resolve short-term hydrological variability, but to capture long-term trends and relative process contributions under climate change. These assumptions make the framework more applicable to lakes and large watersheds with slow turnover, while uncertainties increase in systems dominated by rapid river flow and strong lateral inputs. Regional variability, data sparsity, and unaccounted local processes may contribute to reduced model performance in certain regions.

3. Results

3.1 Meta-analysis of global PAHs concentrations in air, water, and sediment

We collected all the available PAHs concentrations from 1993 to 2021 in air (C_a, n = 290, Table S1, Supplementary Information (SI)), water (C_w, n = 931, Table S2, SI), and sediment (C_s, n = 1,521, Table S3, SI) from the literature for a global meta-analysis, primarily covering three regions:

East Asia (EA, n = 2,074 in three phases), Europe (EU, n = 230), and North America (NA, n = 442) (Fig. 1). During this period, the sum of yearly average C_a of the 16 prioritized PAHs ($\Sigma 16\overline{C}_a$) in NA (4.1-16.1 ng/m^3) was significantly lower than that in EU (8.6-42.3 ng/m^3) and EA (11.8-32.6 ng/m^3) (Fig. 1a-c). The $\Sigma 16\overline{C}_a$ peaked during 2006-2008 and decreased in NA by 71.5% by 2016 and in EU by 79.7% by 2014, while maintained at stable high levels in EA. The medians of $\Sigma 16\overline{C}_a$ in the three regions decreased significantly. These results highlight the positive impact of source PAHs reduction on C_a (Fig. S9 and Tables S10-11, SI), which is driven by regional industrial transformations and relocations, and distinct technical and regulatory controls over PAHs releases [56].

However, the sum of yearly average C_w of the 16 prioritized PAHs ($\Sigma 16\overline{C}_w$) demonstrated disparate temporal profiles than the corresponding $\Sigma 16\overline{C}_a$, particularly in EU. The time-dependent $\Sigma 16\overline{C}_a$ and $\Sigma 16\overline{C}_w$ are poorly correlated in EA ($R^2 = 0.22$, $p > 0.05$), EU ($R^2 = 0.18$, $p > 0.05$), and NA ($R^2 = 0.23$, $p > 0.05$) (Fig. 1a-c and Table S12, SI). The largest gaps are noticed between the $\Sigma 16\overline{C}_a$ and $\Sigma 16\overline{C}_w$ in EA throughout 2001-2017, followed by in EU before 2004 and after 2012. These differences are well anticipated, as individual C_w are influenced by multiple factors besides C_a, such as the PAHs concentrations in sediment (C_s) and site-specific degradation factors [23, 33]. Therefore, we studied three watersheds with more data availability, including the St. Lawrence, the Yangzte, and the Huanghe watersheds, using the OSMF model as a mechanistic diagnostic tool for exploring dominant transport pathways and climate-sensitivity patterns.

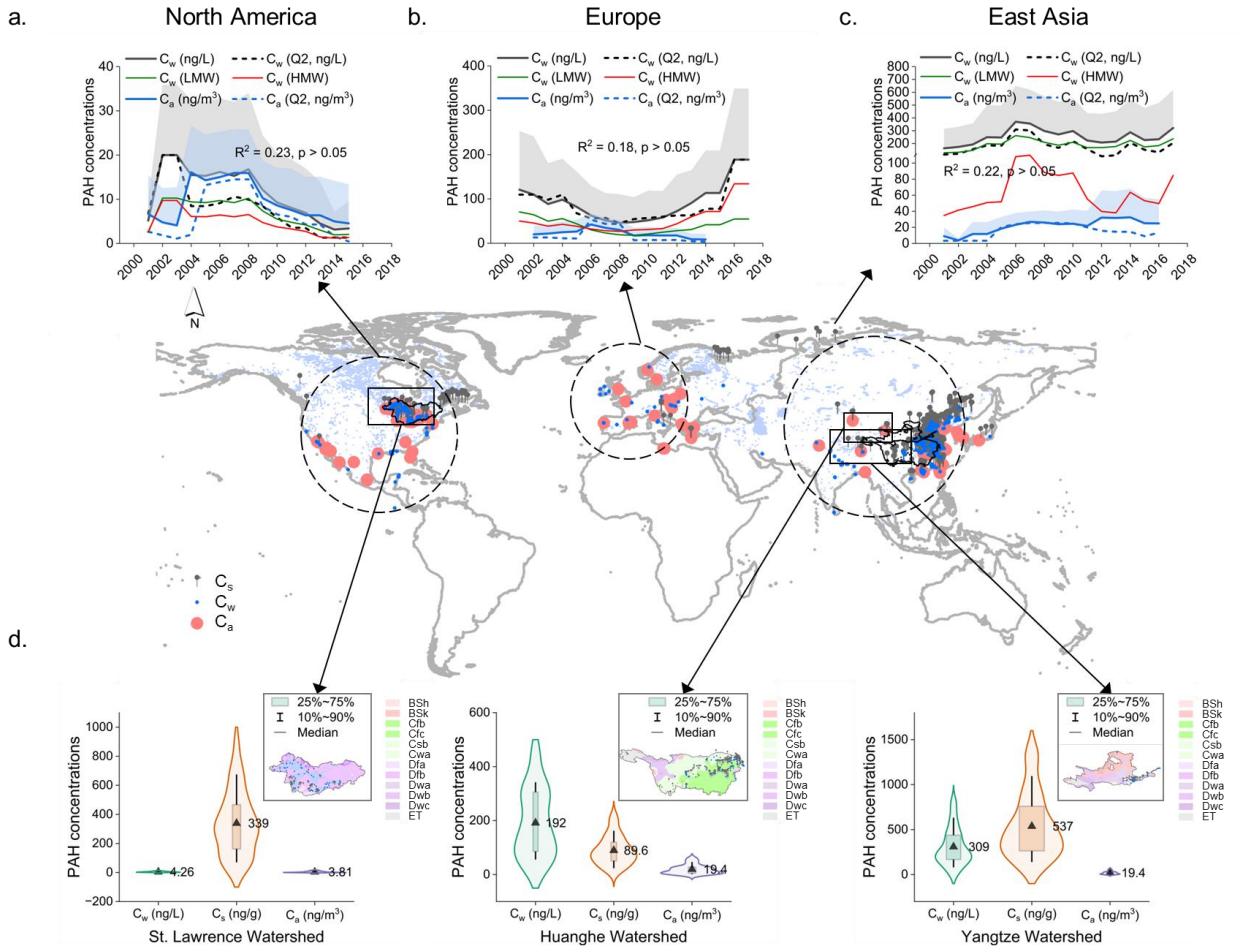

Figure 1: Global PAHs concentrations in air, water, and sediment. a-c. Time-series between 1997-2020 of means (+1 standard deviation (σ)) and medians (50% quantile, Q_2) of sum of yearly average concentrations of the 16 prioritized PAHs in air ($\Sigma_{16}\overline{C}_a$, n = 290), surface water (($\Sigma_{16}\overline{C}_w$, n = 931), and sediment (($\Sigma_{16}\overline{C}_s$, n = 1,521) in North America (NA, n = 442) (a), Europe (EU, n = 230) (b), and East Asia (EA, n= 2,074) (c); d-f. Concentrations of the sum of 16 prioritized PAHs in the St. Lawrence (n = 124, 80, and 133, Fig. 1d) watersheds, Huanghe (n = 78, 56, and 62, Fig. 1e) and Yangtze (n = 78, 171, and 239 in air, water and sediment, respectively, Fig. 1f) between 1996-2021; g-h. Distribution of PAHs measurements in air, water, and sediment in the St. Lawrence, the Yangtze, and the Huanghe watersheds, respectively. The shaded areas stand for the uncertainty ranges of reported data (+1σ). Time-series values are presented as the 5-year moving averages to reduce the influence of outlier values. The concentrations of PAHs in Figs. 1d-f are

plotted as box-and-whiskers, where the line in the box indicates median, the edges of the box are the 25th-75th percentile range, and the whiskers are the 10th-90th range of the interquartile range.

3.2 Divergent fluxes trends of LMW and HMW PAHs in air-water-sediment nexus in three major watersheds

The data availability is highly skewed toward three watersheds: the St. Lawrence watershed in NA (n = 337), and the Huanghe watershed (n = 196) and Yangtze watershed (n = 488) in EA (Fig. 1), which were selected as the subsequent focus of this study. The distribution of $\Sigma 16\overline{C}_w$ in the three watersheds follows the order of Yangtze (308.8 ± 205.0 ng/L) > Huanghe (191.7 ± 126.1 ng/L) > St. Lawrence (4.3 ± 3.3 ng/L), while the sum of yearly average concentrations of the 16 prioritized PAHs in sediment ($\Sigma 16\overline{C}_s$) follows the order of Yangtze (537.3 ± 359.8 ng/g) > St. Lawrence (338.9 ± 219.7 ng/g) > Huanghe (89.6 ± 52.4 ng/g) (Fig. 1a). These values remain at high levels despite emission controls [36], posing threats to public health and aquatic ecosystems. To better understand the causes of disparities between the $\Sigma 16\overline{C}_w$ and $\Sigma 16\overline{C}_s$, it is necessary to consider all the possible PAHs transport pathways and fluxes using static and dynamic models. Various PAHs fluxes were analyzed as inputs to the surface water of each watershed, which is assumed to be a completely mixed waterbody [57]. These fluxes include the F_D (Table S4, SI), F_{AW}, F_{SW}, and F_{GE}. These fluxes are correlated, approaching temporal equilibrium in the air-water-sediment nexus based on the respective equilibrium equations (Fig. S1, SI).

F_D remains the primary pathway for PAHs input [58, 59], with higher values in the Yangtze and Huanghe watersheds compared to the St. Lawrence due to elevated PAHs emissions in China [3, 60, 61]. The total F_D for the 16 prioritized PAHs ($\Sigma 16\overline{C}_D$) is (1.9 ± 2.2) ×10^3, (0.4 ± 0.7) ×10^3, and (0.3 ± 0.3) ×10^3 μg/m^2/year in the Yangtze, Huanghe, and St. Lawrence watershed, respectively (Fig. 2a). Dry deposition contributes 75.8% of F_D (Table S4, SI). HMW PAHs, which are more toxic and particle-affinitive [62], dominate, making up 61.1% and 72.7% of total F_D in the Chinese and St. Lawrence watersheds, respectively (Fig. 2a). PHE is amongst the most abundant congeners across

all watersheds, while some PAHs, including ACY, ANT, BaA, and DahA, contribute minimally [63]. Modelled fluxes show that most LMW PAHs (except NAP, FLU, and PHE in the St. Lawrence) volatilize from water. F_{AW} in the Yangtze and Huanghe watersheds ($(1.4 \pm 0.7) \times 10^4$ and $(5.3 \pm 1.4) \times 10^3$ μg/m^2/year) is 2-3 orders of magnitude higher than in the St. Lawrence (49 ± 42 μg/m^2/year) (Fig. 2a). NAP shows the highest C_w in the Chinese watersheds due to widespread sources [63] and strong solubility [46, 64, 65]. HMW PAHs primarily migrate from air to water, but exceptions exist across watersheds, for instance, HMW PAHs, including FLA, PYR, BaA, BbF, and BaP, volatilize from the aqueous phase into the air in the Yangtze watershed, while LMW PAHs, including NAP, FLU, and PHE, tend to transport into the aqueous phase in the St. Lawrence watershed, influenced by wind speeds (Table S13, SI) and temperature [66, 67], which impact volatilization.

F_{SW}, assessed via Fick's law [68] (Equations 10-12), shows sediment act as a major sink for 13 out of 16 PAHs in the Yangtze and Huanghe watersheds, but a net source in the St. Lawrence (Fig. 2a). The St. Lawrence F_{SW} ($(3.6 \pm 1.5) \times 10^4$ μg/m^2/year) is 4 times higher than in the Yangtze and Huanghe watersheds (Fig. 2a). NAP dominates sediment fluxes across all watersheds, though high uncertainties exist due to fluctuating PAHs concentrations. F_{GE}, modelled via bubble adsorption/partitioning [19] (Equations 13-15), is 2-3 orders of magnitude lower than F_{AW} and F_{SW} in the Yangtze and Huanghe, but in the St. Lawrence, it is comparable to F_D and much higher than F_{AW}. Total F_{GE} in the St. Lawrence (434 ± 253 μg/m²/year) significantly exceeds that of the Yangtze and Huanghe watersheds (27.9 ± 13.3 μg/m²/year) due to the lower C_s (Fig. 2a). HMW PAHs dominate F_{GE} in the Yangtze and St. Lawrence watersheds. Overall, PAHs exchanges at the air-water and water-sediment interfaces are mainly controlled by F_{AW} and F_{SW}. Sediment can act as a PAHs source or sink, depending on equilibrium conditions. F_{SW} can counterbalance F_{AW} in East Asia when flux directions are opposite. Notably, F_{GE} is minor in the Yangtze and Huanghe watersheds but significant in the St. Lawrence, where F_D remains the dominant PAHs input pathway.

3.3 Predicted PAHs distributions in three major watersheds by 2050 under climate change

Historical PAHs emissions were driven by various factors linked with socioeconomic contexts, such as energy consumption, population, technology, and GDP [69-72]. Technology advancements [3, 73] coupled with increased social awareness [74, 75] have significantly inhibited PAHs emissions. To predict regional PAHs emissions between 2021-2050, we utilized a constant elasticity of substitution (CES) model (Equation 16), correlating typical socioeconomic factors, including energy consumption (Fig. S10, SI) and GDP (Fig. S11, SI) under three selected shared socioeconomic pathways (SSPs) [76], including SSP1, SSP2, and SSP5, to understand the influence of various developments in global society and economy (Fig. S12, SI). In NA, the PAHs emissions are projected to be reduced by 64% by 2050, nearly double the reduction percentage in EA (Fig. S9, SI). The regional changes in PAHs emissions will significantly impact their presences in the watersheds.

We predicted future aqueous PAHs concentrations using a OSMF model combined with time-dependent PAHs emissions, degradation, and climate change. Climate change has significant implications for environmental chemistry of PAHs. Critical parameters like Henry's law constant (H), the octanol-water partition coefficient (K_{ow}), and the air-water partition coefficient (K_{aw}) all influence the environmental fate, transport, and bioavailability of PAHs, which are temperature-dependent. As temperatures rise, the solubility of PAHs in water tends to decrease, leading to an increase in H, which causes more PAHs to volatilize from aquatic environments into the atmosphere (Fig. S5, SI). Furthermore, climate change also alters the partitioning behavior of PAHs between sediment and water, likely enhance their mobility in sediment (Fig. S6, SI). Given the abundance of PAHs in sediment and their high sensitivity to temperature [19], we expect F_{GE} to gradually increase in the future [19, 77]. However, trends of F_D are uncertain due to conflicting factors: while global efforts to reduce PAHs emissions should decrease F_D, the increasing frequency of extreme weather events caused by climate change could drive F_D upward.

Under the baseline scenario without climate change, $\Sigma 16C_w$ in the Yangtze, Huanghe, and St. Lawrence watersheds are expected to decline by 47.6%, 8.7%, and 19.4%, respectively, from 2021 levels by 2026, followed by additional reductions of 13.8%, 9.7%, and 19.7%, respectively, by 2050 (Fig. S13, SI). These reductions are primarily due to the volatilization of LMW PAHs into the air through air-water exchange (Fig. 2b). Conversely, the Huanghe watershed will experience a rapid increase in HMW C_w from 53.3 ng/L to 105.8 ng/L by 2030, which will then plateau. Meanwhile, the HMW C_w in the Yangtze (82.5 ± 66.0 ng/L) and St. Lawrence (3.2 ± 2.8 ng/L) watersheds will remain largely stable until 2050 (Fig. 2c). This is due to the combined effects of atmospheric deposition, air-water exchange, and bubble ebullition, which favor the accumulation of HMW PAHs in the aqueous phase.

Under integrated climate-change scenarios that combine SSP with greenhouse-gas concentration trajectories (Representative Concentration Pathways, RCPs) – specifically SSP1-RCP2.6 (SSP126), SSP2-RCP4.5 (SSP245), and SSP5-RCP8.5 (SSP585). C_w is expected to rebound from 169-171 ng/L in 2026 to 236-256 ng/L by 2050 in the Yangtze watershed and from 152-155 in 2026 to 150-176 ng/L by 2050 in the Huanghe watershed, with the highest C_w observed under SSP585 (Fig. S13, SI), attributed to accelerated fossil fuel usage. Both LMW (27.3-75.4%, Fig. 2b) and HMW (24.6-72.7%, Fig. 2c) PAHs will contribute to these increased C_w levels. Certain congeners, such as BBF, ANT, and PHE, will account for 30% and 29% of $\Sigma 16C_w$ in the Yangtze and Huanghe watersheds, respectively (Fig. 2d, e). Climate change will significantly increase the C_w of BBF, ANT, and PHE in the Yangtze watershed by 84.4-89.3 ug/L, 14.5-16.8 ug/L, and 12.1-15.3 ug/L, respectively, by 2050, mainly due to sediment diffusion. The impact of climate change on the St. Lawrence watershed is expected to be minimal due to high degradation rates that counteract the accumulation of most congeners (Table S5, SI). As C_w and C_a dynamically change under climate influences, most LMW PAHs will significantly decrease in the sediment. NAP and ACE will nearly deplete by 2050 in all the watersheds (Fig. 2g-i). However, HMW PAHs will accumulate in the EA watersheds, with the C_s of BBF increasing by up to 10 ug/L in the Yangtze

watershed (Fig. 2g). This highlights the sediment as intermediate sink for HMW PAHs despite global emission reductions.

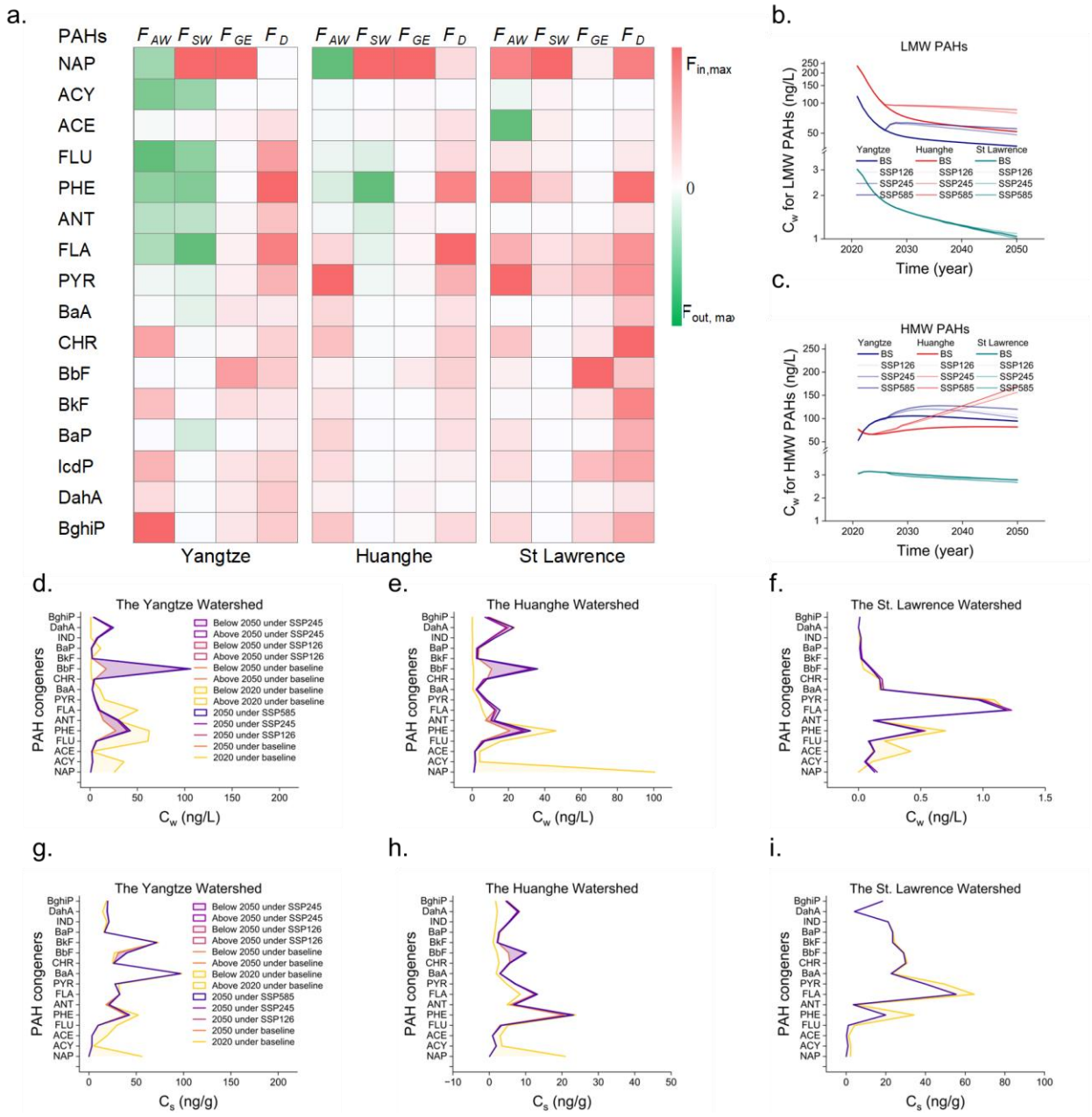

Figure 2: Predicted PAHs concentrations in surface water and sediment by 2050. a. Monte Carlo simulated temporary air-water exchange (F_{AW}), air deposition (F_D), sediment-water diffusion (F_{SW}), and bubble ebullition-facilitated flux (F_{GE}) in the Yangtze, Huanghe, and St. Lawrence watersheds,

respectively, under the initial boundary PAHs based on Fig. S1 (SI). Positive values indicate PAHs fluxes moving into water phase, and vice versa; b-c. Predictions for the concentrations of LMW PAHs (Fig. 2b) and HMW PAHs (Fig. 2c) in the surface water of the Yangtze (YZ), Huanghe (HH), and St. Lawrence (SL) watersheds under baseline (BS) and climate change scenarios (SSP126, SSP245, and SSP585). The climate change scenarios are represented by various Shared Socioeconomic Pathways (SSPs, including SSP1, SSP2, and SSP5) coupled with Representative Concentration Pathways (RCPs, including RCP2.6, RCP4.5, and RCP8.5), entitled SSP126, SSP245, and SSP585, as recommended by the Intergovernmental Panel for Climate Change (IPCC); d-f. predictions for the C_w of 16 PAHs in the Yangtze (Fig. 2d), Huanghe (Fig. 2e), and St. Lawrence (Fig. 2f) watersheds under baseline and climate change scenarios; g-i. predictions for the C_s of 16 PAHs in the Yangtze (Fig. 2g), Huanghe (Fig. 2h), and St. Lawrence (Fig. 2i) watersheds under baseline and climate change scenarios.

3.4 Increased risk of aqueous HMW PAHs by 2050 under climate change

Under the baseline scenario, the total risks for algae, crustaceans, and fish (ΣRQs) between 2021-2050 in the Yangtze and Huanghe watersheds are 9.4-14.3 and 8.2-19.8, respectively, both peaking during 2030-2040. These values are 55-136 and 63-102 times higher than those in the St. Lawrence watershed (0.13-0.15), respectively (Fig. 3a-c). Throughout 2021-2050, PAHs present moderate risks to surface water in EA with the most risk on algal populations (81-89% of ΣRQs, Fig. 3a-c), to which IcdP (RQ = 5-14 to the algae) is the main contributor. The risks to EA's crustaceans and fish are of no concern. Under SSP585, the ΣRQs between 2021-2050 in the St. Lawrence watershed (0.13-0.15) remain at a low level (Fig. 3f), similar to that under the baseline scenario (Fig. 3c), attributing to high degradation factors. However, ΣRQs significantly increase in the Yangtze watershed by 31-56% between 2040-2050 (Fig. 3d). Under climate change scenarios, the Huanghe watershed also experiences increased ΣRQs by >10% since 2035 (Fig. 3b, e). These trends align with potential risk assessments based on inter-regional multimedia fate analysis of

PAHs [78]. The increases in ΣRQs in EA by 2050 are mainly contributed by sediment input through F_{SW}. The replenishment of BbF to surface water under SSP585 is mainly responsible for 30-79% and 77-80% of the increased ΣRQs by 2050 in the Yangtze and Huanghe watersheds, respectively (Fig. 3d, e). However, the risk induced by IcdP remains dominant, accounting for 69-80% of the ΣRQs in EA's watersheds.

Under the baseline scenario, the trend of ΣTEQs is consistent with that of ΣRQs. The ΣTEQs in the EA's watersheds are 106-362 times higher than that in the St. Lawrence watershed by 2050 (Fig. 3g-i). The ΣTEQs in the Yangtze (0.06-0.11 nM) and Huanghe (0.04-0.11 nM) watersheds are expected to increase by 99% and 192%, respectively, between 2021-2050, while decrease by 10% in the St. Lawrence watershed ($3.2\text{-}3.6\times10^{-4}$ nM) (Fig. 3g-l). BaP (0.009-0.018 nM) and DahA (0.020-0.091 nM) are the primary contributors in EA, together accounting for 75-89% and 78-88% of ΣTEQs between 2021-2050 in the Yangtze and Huanghe watersheds, respectively. CHR ($8.2\text{-}8.9\times10^{-5}$ nM, 24-26%), BaA ($7.9\text{-}8.4\times10^{-5}$ nM, 23-25%), BaP ($6.3\text{-}6.9\times10^{-5}$ nM, 19-20%), and BbF ($3.6\text{-}4.0\times10^{-5}$ nM, 10-12%) are the top four congeners contributing to ΣTEQs in the St. Lawrence watershed (Fig. 3i). By 2050 under SSP585, ΣTEQs are 32% and 5% higher in the Huanghe and Yangtze watersheds, respectively, compared to the baseline scenario, but 4% lower in the St. Lawrence watershed (Fig. 3g-l). The temporal variations in congeners' TEQs and their contributions to ΣTEQs are expected due to climate change impacts. For example, under SSP585, the TEQs of BbF and DahA will increase by 48% and 192% in the Huanghe watershed but remain steady in the Yangtze watershed and decrease by 18% in the St. Lawrence watershed by 2050 (Fig. 3j-i). Fortunately, the ΣTEQs [54] of all the surface water in the watersheds will be within the acceptable range recommended by the United States Environmental Protection Agency (USEPA). However, the surface water in EA by 2050 may suffer from potential carcinogenic toxicity if gauged by the standards set by the Swedish Environmental Protection Agency and the Royal Society of UK [79].

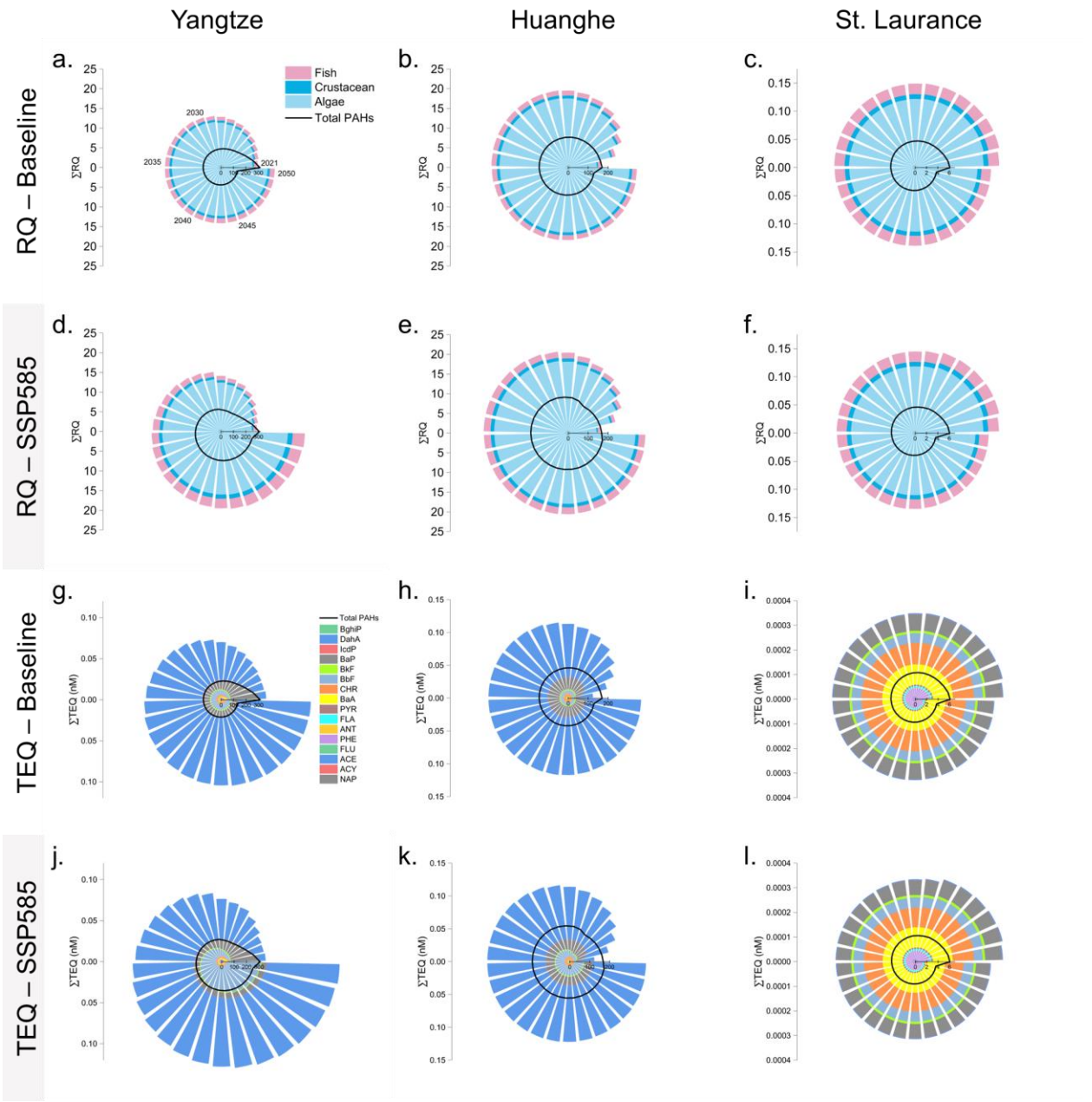

Figure 3: Predicted PAHs risks in surface water by 2050. a-f. Predictions of ecological risks of the PAHs represented by Risk Quotient (RQ) from 2021 to 2050 (counter-clockwise order) in the Yangtze (a, d), Huanghe (b, e), and St. Lawrence (c, f) watersheds under baseline (a-c) and SSP585 scenario (d-f), respectively; g-l. predictions of carcinogenic toxicity of the PAHs represented by Dioxin Toxicity Equivalence (TEQ) from 2021 to 2050 (counter-clockwise order) in the Yangtze

(g, j), Huanghe (h, k), and St. Lawrence (i, l) watersheds under baseline (g-i) and SSP585 scenario (j-l), respectively. The predicted $\Sigma 16C_w$ is plotted in Fig. 3a-l for comparison.

4. Discussion and conclusions

Our study highlights the persistence of HMW PAHs such as FLA, BbF, and DahA in surface water, despite global reductions in PAHs emissions. This persistence is particularly concerning for the watersheds in EA, where these pollutants are expected to contribute to long-term moderate ecological risks until 2050. In contrast, the St. Lawrence watershed is expected to experience low ecological risk, primarily ascribed to higher degradation factors that reduce PAHs concentrations. The sediment in these watersheds emerges as a major PAHs source to surface waters, emphasizing the need for targeted strategies to manage these inputs. In the EA watersheds, IcdP is identified as the main contributor to aquatic ecological risks with respect to ΣRQs, while BbF, BaP and DahA dominate ΣTEQs. This profile contrasts with the St. Lawrence watershed, where Fla, Pyr, BaA and IcdP are the dominant contributors to ΣRQs, and BaA, CHR, BhF, and BaP dominate ΣTEQs. Notably, climate change may significantly reshape or even intensify ecological risks profiles by altering interfacial fluxes. For instance, enhanced input of BbF into EA's surface water—by as much as 33-524% between 2030 and 2050—will likely increase its contribution to ΣRQs from 3-7% to 7-28% and to ΣTEQs from 4-8% to 9-29%. These findings emphasize the importance of managing sediment as a critical source of PAHs to surface water. While emission controls are essential, they are insufficient on their own to eliminate PAHs from surface water without addressing sediment inputs.

The regional disparity in PAHs emission intensity further complicates the picture (Fig. S10, SI). Asia, as the largest consumer of fossil fuels, exhibits a higher average PAHs emission intensity (0.02 t/ktoe) compared to EU (0.01 t/ktoe) and NA (0.003 t/ktoe), where advanced power generation technologies prevail (Fig. S10, SI). These disparities underscore the necessity for region-specific strategies to address PAHs accumulation in surface water. Moreover, the global

shift towards renewable and alternative fuels, including biomass, could emerge as a new significant source of PAHs emissions [1]. Our watershed-scale analysis reveals that aqueous PAHs will continue to pose ecological and health risks over time, regardless of global PAHs emission reductions. Addressing PAHs pollution in surface water requires a multi-faceted approach that includes tailored controls and treatments of both surface water and sediment. Natural monitored attenuation may be effective in lightly to moderately polluted areas, while more aggressive interventions—such as capping [80], stabilization, dredging, physicochemical sorption [81], thermal desorption, flushing, and enhanced biodegradation [82] are necessary for heavily polluted sediment hotspots and water sources crucial for human livelihoods [83].

The variability in PAHs emission intensities across regions, coupled with the impacts of climate change, presents challenges for predicting future PAHs distributions and risks in surface water. The complexities of PAHs sources and the changing climate underscore the need for a comprehensive understanding of PAHs migration and degradation processes across air, water, and sediment, as well as their ecotoxicities in global ecosystems. However, data scarcity, particularly in emerging economies like India, and South American and African countries, hampers a comprehensive global assessment of PAHs transport, fate, and associated risks. Economic developments coupled with demographic booming in these regions may indicate lags in potential PAHs ecotoxicities being noted from watersheds in developed regions. For many watersheds which are not scrutinized in the study, for instance those in EU and other areas in EA, their PAHs in surface water may likely follow a similar trend from the Yangtze and Huanghe watersheds, given degradation factors among these regions are not high (Table S5, SI). This study also recognizes the potential interactions between PAHs and other persistent organic pollutants (POPs) in sediment, which could exacerbate overall risks in surface water.

Given these challenges, future research should prioritize understanding transformation mechanisms and interactive toxicity in ecosystems. Innovations in technology and management strategies for PAHs emission reduction and remediation are crucial. Policymakers need to integrate

scientific advancements with adaptive environmental regulations, promoting pilot- and full-scale projects aligned with the Sustainable Development Goals (SDG) target 6.3. Additionally, there are significant uncertainties in predicting surface-water PAHs concentrations, particularly when considering sediment PAHs concentrations and degradation factors. Comprehensive field monitoring is needed to validate these predictions.

Acknowledgement

None.

Author contribution statement

Tingting Sun: Data curation, Formal analysis, Writing – original draft. Mingliang Fang: Conceptualization, Investigation, Writing – review & editing. Jingyu Zhu: Methodology, Writing – review & editing. Lusha Zeng: Analysis, Visualization, Methodology, Writing – review & editing. Fanrong Zhao: Analysis, Visualization, Writing – review & editing. Changzhi Shi: Analysis, Visualization, Writing – review & editing. Shuhan Ren: Writing – review & editing. Ke Yin: Conceptualization, Investigation, Writing – original draft, Project administration. Qianhong She: Writing – review & editing. Xunchang Fei: Conceptualization, Method, Validation, Writing – review & editing.

Data availability

The data that support the findings of this study are included in the article or supplementary materials.

Declaration of competing interest

All the contributing authors report no conflicts of interest in this work.

Funding

This work is granted by the National Key Research and Development Program of China (Grant No. 2024YFA0918900), Singapore Ministry of Education, and Nanjing Forestry University.

Use of AI statement

None.

Electronic Supplementary Material: Supplementary material is available in the online version of this article at https://doi.org/10.26599/CS.2026.9510007

References

1. González-Gaya, B.; Fernández-Pinos, M.-C.; Morales, L.; Méjanelle, L.; Abad, E.; Piña, B.; Duarte, C. M.; Jiménez, B.; Dachs, J., High atmosphere–ocean exchange of semivolatile aromatic hydrocarbons. *Nature Geoscience* **2016,** *9* (6), 438-442.
2. Li, L.; Chen, C.; Li, D.; Breivik, K.; Abbasi, G.; Li, Y.-F., What do we know about the production and release of persistent organic pollutants in the global environment? *Environmental Science: Advances* **2023,** *2* (1), 55-68.
3. Shen, H.; Huang, Y.; Wang, R.; Zhu, D.; Li, W.; Shen, G.; Wang, B.; Zhang, Y.; Chen, Y.; Lu, Y.; Chen, H.; Li, T.; Sun, K.; Li, B.; Liu, W.; Liu, J.; Tao, S., Global Atmospheric Emissions of Polycyclic Aromatic Hydrocarbons from 1960 to 2008 and Future Predictions. *Environmental Science & Technology* **2013,** *47* (12), 6415-6424.
4. Du, J.; Jing, C., Anthropogenic PAHs in lake sediments: a literature review (2002–2018). *Environmental Science: Processes & Impacts* **2018,** *20* (12), 1649-1666.
5. Tulcan, R. X. S.; Liu, L.; Lu, X.; Ge, Z.; Fernández Rojas, D. Y.; Mora Silva, D., PAHs contamination in ports: Status, sources and risks. *Journal of Hazardous Materials* **2024,** *475*, 134937.
6. Zhang, M.; Tang, Z.; Yin, H.; Meng, T., Concentrations, distribution and risk of polycyclic aromatic hydrocarbons in sediments from seven major river basins in China over the past 20 years. *Journal of Environmental Management* **2021,** *280*, 111717.
7. Castro-Jiménez, J.; Berrojalbiz, N.; Wollgast, J.; Dachs, J., Polycyclic aromatic hydrocarbons (PAHs) in the Mediterranean Sea: Atmospheric occurrence, deposition and decoupling with settling fluxes in the water column. *Environmental pollution* **2012,** *166*, 40-47.
8. Del Vento, S.; Dachs, J.; technology, Atmospheric occurrence and deposition of polycyclic aromatic hydrocarbons in the northeast tropical and subtropical Atlantic Ocean. *Environmental Pollution* **2007,** *41* (16), 5608-5613.
9. Tamamura, S.; Sato, T.; Ota, Y.; Aota, Y.; Kashiwaya, K.; Kumagai, M., Seasonal Deposition Fluxes of Polycyclic Aromatic Hydrocarbons (PAHs) in Lake Biwa, Japan. *Water Air and Soil Pollution* **2009,** *198* (1-4), 297-306.
10. Tucca, F.; Luarte, T.; Nimptsch, J.; Woelfl, S.; Pozo, K.; Casas, G.; Dachs, J.; Barra, R.; Chiang, G.; Galbán-Malagón, C., Sources and diffusive air–water exchange of polycyclic aromatic hydrocarbons in an oligotrophic North–Patagonian lake. *Science of The Total Environment* **2020,** *738*, 139838.
11. Jiang, Y.; Lin, T.; Wu, Z.; Li, Y.; Li, Z.; Guo, Z.; Yao, X., Seasonal atmospheric deposition and air–sea gas exchange of polycyclic aromatic hydrocarbons over the Yangtze River Estuary, East China Sea: Implications for source–sink processes. *Atmospheric Environment* **2018,** *178*, 31-40.
12. Rasiq, K. T.; El-Maradny, A.; Orif, M.; Bashir, M. E.; Turki, A. J., Polycyclic aromatic hydrocarbons in two polluted lagoons, eastern coast of the Red Sea: Levels, probable sources,

dry deposition fluxes and air-water exchange. *Atmospheric Pollution Research* **2019,** *10* (3), 880-888.

13. Li, J.; Cheng, H.; Zhang, G.; Qi, S.; Li, X., Polycyclic aromatic hydrocarbon (PAH) deposition to and exchange at the air–water interface of Luhu, an urban lake in Guangzhou, China. *Environmental Pollution* **2009,** *157* (1), 273-279.

14. Wang, D.-G.; Alaee, M.; Byer, J.; Liu, Y.-J.; Tian, C.-G., Fugacity approach to evaluate the sediment-water diffusion of polycyclic aromatic hydrocarbons. *Journal of Environmental Monitoring* **2011,** *13* (6), 1589-1596.

15. Cui, S.; Fu, Q.; Li, T.-x.; Ma, W.-l.; Liu, D.; Wang, M., Sediment-Water Exchange, Spatial Variations, and Ecological Risk Assessment of Polycyclic Aromatic Hydrocarbons (PAHs) in the Songhua River, China. *Water* **2016,** *8* (8).

16. Koelmans, A. A.; Poot, A.; De Lange, H. J.; Velzeboer, I.; Harmsen, J.; van Noort, P. C. M., Estimation of In Situ Sediment-to-Water Fluxes of Polycyclic Aromatic Hydrocarbons, Polychlorobiphenyls and Polybrominated Diphenylethers. *Environmental Science & Technology* **2010,** *44* (8), 3014-3020.

17. Sabin, L. D.; Maruya, K. A.; Lao, W.; Diehl, D.; Tsukada, D.; Stolzenbach, K. D.; Schiff, K. C.; Chemistry, Exchange of polycyclic aromatic hydrocarbons among the atmosphere, water, and sediment in coastal embayments of southern California, USA. *Environmental Toxicology* **2010,** *29* (2), 265-274.

18. Fernandez, L. A.; Lao, W.; Maruya, K. A.; Burgess, R. M., Calculating the Diffusive Flux of Persistent Organic Pollutants between Sediments and the Water Column on the Palos Verdes Shelf Superfund Site Using Polymeric Passive Samplers. *Environmental Science & Technology* **2014,** *48* (7), 3925-3934.

19. Sun, T.; Li, W.; Yin, K., Estimation of total flux of polycyclic aromatic hydrocarbons facilitated by methane ebullition into water column from global lake sediments. *Water Research* **2021,** *204*, 117611.

20. Viana, P. Z.; Yin, K.; Rockne, K. J., Field Measurements and Modeling of Ebullition-Facilitated Flux of Heavy Metals and Polycyclic Aromatic Hydrocarbons from Sediments to the Water Column. *Environmental Science & Technology* **2012,** *46* (21), 12046-12054.

21. Viana, P.; Yin, K.; Rockne, K., Comparison of direct benthic flux to ebullition-facilitated flux of polycyclic aromatic hydrocarbons and heavy metals measured in the field. *Journal of Soils and Sediments* **2018,** *18* (4), 1729-1742.

22. Cao, Y.; Wang, J.; Xin, M.; Wang, B.; Lin, C., Spatial distribution and partition of polycyclic aromatic hydrocarbons (PAHs) in the water and sediment of the southern Bohai Sea: Yellow River and PAH property influences. *Water Research* **2024,** *248*, 120873.

23. Xu, F.-L.; Qin, N.; Zhu, Y.; He, W.; Kong, X.-Z.; Barbour, M. T.; He, Q.-S.; Wang, Y.; Ou-Yang, H.-L.; Tao, S., Multimedia fate modeling of polycyclic aromatic hydrocarbons (PAHs) in Lake Small Baiyangdian, Northern China. *Ecological Modelling* **2013,** *252*, 246-257.

24. Arhami, M.; Minguillón, M. C.; Polidori, A.; Schauer, J. J.; Delfino, R. J.; Sioutas, C., Organic compound characterization and source apportionment of indoor and outdoor quasi-ultrafine particulate matter in retirement homes of the Los Angeles Basin. *Indoor Air* **2010,** *20* (1), 17-30.
25. Cui, H.; Lu, Y.; Zhou, Y.; He, G.; Li, Q.; Liu, C.; Wang, R.; Du, D.; Song, S.; Cheng, Y., Spatial variation and driving mechanism of polycyclic aromatic hydrocarbons (PAHs) emissions from vehicles in China. *Journal of Cleaner Production* **2022,** *336*, 130210.
26. Birgul, A.; Tasdemir, Y., Concentrations, Gas-Particle Partitioning, and Seasonal Variations of Polycyclic Aromatic Hydrocarbons at Four Sites in Turkey. *Archives of Environmental Contamination and Toxicology* **2015,** *68* (1), 46-63.
27. Marquès, M.; Mari, M.; Sierra, J.; Nadal, M.; Domingo, J. L., Solar radiation as a swift pathway for PAH photodegradation: A field study. *Science of The Total Environment* **2017,** *581-582*, 530-540.
28. Borrowman, C. K.; Zhou, S.; Burrow, T. E.; Abbatt, J. P. D., Formation of environmentally persistent free radicals from the heterogeneous reaction of ozone and polycyclic aromatic compounds. *Physical Chemistry Chemical Physics* **2016,** *18* (1), 205-212.
29. Kwamena, N. O. A.; Abbatt, J. P. D., Heterogeneous nitration reactions of polycyclic aromatic hydrocarbons and n-hexane soot by exposure to NO3/NO2/N2O5. *Atmospheric Environment* **2008,** *42* (35), 8309-8314.
30. Tomaz, S.; Shahpoury, P.; Jaffrezo, J.-L.; Lammel, G.; Perraudin, E.; Villenave, E.; Albinet, A., One-year study of polycyclic aromatic compounds at an urban site in Grenoble (France): Seasonal variations, gas/particle partitioning and cancer risk estimation. *Science of The Total Environment* **2016,** *565*, 1071-1083.
31. Odabasi, M.; Sofuoglu, A.; Vardar, N.; Tasdemir, Y.; Holsen, T. M., Measurement of Dry Deposition and Air−Water Exchange of Polycyclic Aromatic Hydrocarbons with the Water Surface Sampler. *Environmental Science & Technology* **1999,** *33* (3), 426-434.
32. Huang, L.; Batterman, S. A., Multimedia Model for Polycyclic Aromatic Hydrocarbons (PAHs) and Nitro-PAHs in Lake Michigan. *Environmental Science & Technology* **2014,** *48* (23), 13817-13825.
33. González-Gaya, B.; Martínez-Varela, A.; Vila-Costa, M.; Casal, P.; Cerro-Gálvez, E.; Berrojalbiz, N.; Lundin, D.; Vidal, M.; Mompeán, C.; Bode, A.; Jiménez, B.; Dachs, J., Biodegradation as an important sink of aromatic hydrocarbons in the oceans. *Nature Geoscience* **2019,** *12* (2), 119-125.
34. McDonough, C. A.; Khairy, M. A.; Muir, D. C. G.; Lohmann, R., Significance of Population Centers As Sources of Gaseous and Dissolved PAHs in the Lower Great Lakes. *Environmental Science & Technology* **2014,** *48* (14), 7789-7797.
35. Chiou, C. T.; McGroddy, S. E.; Kile, D. E., Partition Characteristics of Polycyclic Aromatic Hydrocarbons on Soils and Sediments. *Environmental Science & Technology* **1998,** *32* (2), 264-269.

36. Wang, W.; Xu, J.; Qu, X.; Lin, D.; Yang, K., Current and Future Trends of Low and High Molecular Weight Polycyclic Aromatic Hydrocarbons in Surface Water and Sediments of China: Insights from Their Long-Term Relationships between Concentrations and Emissions. *Environmental Science & Technology* **2022,** *56* (6), 3397-3406.
37. Cheung, M. W. L.; Vijayakumar, R., A Guide to Conducting a Meta-Analysis. *Neuropsychology Review* **2016,** *26* (2), 121-128.
38. Parnis, J. M.; Mackay, D., *Multimedia Environmental Models: The Fugacity Approach*. CRC Press: 2020.
39. Gurevitch, J.; Koricheva, J.; Nakagawa, S.; Stewart, G., Meta-analysis and the science of research synthesis. *Nature* **2018,** *555* (7695), 175-182.
40. Shi, X.; Mao, D.; Song, K.; Xiang, H.; Li, S.; Wang, Z., Effects of landscape changes on water quality: A global meta-analysis. *Water Research* **2024,** *260*, 121946.
41. Xu, Y.; Zhang, Y.-L.; Li, J.; Gioia, R.; Zhang, G.; Li, X.-D.; Spiro, B.; Bhatia, R. S.; Jones, K. C., The spatial distribution and potential sources of polycyclic aromatic hydrocarbons (PAHs) over the Asian marginal seas and the Indian and Atlantic Oceans. *Journal of Geophysical Research: Atmospheres* **2012,** *117* (D07302), 1-10.
42. Duce, R. A.; Liss, P. S.; Merrill, J. T.; Atlas, E. L.; Buat-Menard, P.; Hicks, B. B.; Miller, J. M.; Prospero, J. M.; Arimoto, R.; Church, T. M.; Ellis, W.; Galloway, J. N.; Hansen, L.; Jickells, T. D.; Knap, A. H.; Reinhardt, K. H.; Schneider, B.; Soudine, A.; Tokos, J. J.; Tsunogai, S.; Wollast, R.; Zhou, M., The atmospheric input of trace species to the world ocean. *Global Biogeochemical Cycles* **1991,** *5* (3), 193-259.
43. Travis, C. C.; Obenshain, K. R.; Regens, J. L.; Whipple, C. G., Limitations of Multimedia Models for Use in Environmental Decision Making. *Environmental Monitoring and Assessment* **2001,** *71* (1), 51-60.
44. Wania, F.; Axelman, J.; Broman, D., A review of processes involved in the exchange of persistent organic pollutants across the air–sea interface. *Environmental Pollution* **1998,** *102* (1), 3-23.
45. Singh, V.; Xu, C. Y., Evaluation and generalization of 13 mass‐transfer equations for determining free water evaporation. *Hydrological Processes* **1997,** *11* (3), 311-323.
46. Qin, N.; He, W.; Kong, X.-Z.; Liu, W.-X.; He, Q.-S.; Yang, B.; Ouyang, H.-L.; Wang, Q.-M.; Xu, F.-L., Atmospheric partitioning and the air–water exchange of polycyclic aromatic hydrocarbons in a large shallow Chinese lake (Lake Chaohu). *Chemosphere* **2013,** *93* (9), 1685-1693.
47. Fang, M.-D.; Lee, C.-L.; Jiang, J.-J.; Ko, F.-C.; Baker, J. E., Diffusive exchange of PAHs across the air–water interface of the Kaohsiung Harbor lagoon, Taiwan. *Journal of Environmental Management* **2012,** *110*, 179-187.
48. He, J.; Balasubramanian, R., The exchange of SVOCs across the air-sea interface in Singapore's coastal environment. *Atmospheric Chemistry and Physics* **2010,** *10* (4), 1837-1852.

49. Bidleman, T. F.; McConnell, L. L., A review of field experiments to determine air-water gas exchange of persistent organic pollutants. *Science of The Total Environment* **1995,** *159* (2-3), 101-117.
50. Wang, J.-Z.; Zhu, C.-Z.; Chen, T.-H., PAHs in the Chinese environment: levels, inventory mass, source and toxic potency assessment. *Environmental Science: Processes & Impacts* **2013,** *15* (6), 1104-1112.
51. Fendinger, N. J.; Adams, D. D.; Glotfelty, D. E., The role of gas ebullition in the transport of organic contaminants from sediments. *Science of The Total Environment* **1992,** *112* (2-3), 189-201.
52. Hoff, J. T.; Mackay, D.; Gillham, R.; Shiu, W. Y., Partitioning of organic chemicals at the air-water interface in environmental systems. *Environmental Science & Technology* **1993,** *27* (10), 2174-2180.
53. Escher, B. I.; Aït-Aïssa, S.; Behnisch, P. A.; Brack, W.; Brion, F.; Brouwer, A.; Buchinger, S.; Crawford, S. E.; Du Pasquier, D.; Hamers, T.; Hettwer, K.; Hilscherová, K.; Hollert, H.; Kase, R.; Kienle, C.; Tindall, A. J.; Tuerk, J.; van der Oost, R.; Vermeirssen, E.; Neale, P. A., Effect-based trigger values for in vitro and in vivo bioassays performed on surface water extracts supporting the environmental quality standards (EQS) of the European Water Framework Directive. *Science of The Total Environment* **2018,** *628-629*, 748-765.
54. Meng, Y.; Liu, X.; Lu, S.; Zhang, T.; Jin, B.; Wang, Q.; Tang, Z.; Liu, Y.; Guo, X.; Zhou, J.; Xi, B., A review on occurrence and risk of polycyclic aromatic hydrocarbons (PAHs) in lakes of China. *Science of The Total Environment* **2019,** *651*, 2497-2506.
55. Cheng, K.; Li, J.-Y.; Wang, Y.; Ji, W.-W.; Cao, Y., Characterization and Risk Assessment of Airborne Polycyclic Aromatic Hydrocarbons From Open Burning of Municipal Solid Waste. *Frontiers in Environmental Science* **2022**, 382.
56. Ramesh, A.; Archibong; Hood, D.; Guo, Z.; Loganathan, B., Global Environmental Distribution and Human Health Effects of Polycyclic Aromatic Hydrocarbons. In *Global Contamination Trends of Persistent Organic Chemicals*, 1st ed.; Loganathan, B. G.; Lam, P. K.-S., Eds. CRC Press: Boca Raton, 2011; pp 97-128.
57. Yu, H.; Liu, Y.; Han, C.; Fang, H.; Weng, J.; Shu, X.; Pan, Y.; Ma, L., Polycyclic aromatic hydrocarbons in surface waters from the seven main river basins of China: Spatial distribution, source apportionment, and potential risk assessment. *Science of The Total Environment* **2021,** *752*, 141764.
58. Liu, F.; Xu, Y.; Liu, J.; Liu, D.; Li, J.; Zhang, G.; Li, X.; Zou, S.; Lai, S., Atmospheric deposition of polycyclic aromatic hydrocarbons (PAHs) to a coastal site of Hong Kong, South China. *Atmospheric Environment* **2013,** *69*, 265-272.
59. Bae, S. Y.; Yi, S. M.; Kim, Y. P., Temporal and spatial variations of the particle size distribution of PAHs and their dry deposition fluxes in Korea. *Atmospheric Environment* **2002,** *36* (35), 5491-5500.

60. Xu, S. S.; Liu, W. X.; Tao, S., Emission of polycyclic aromatic hydrocarbons in China. *Environmental Science & Technology* **2006,** *40* (3), 702-708.
61. Zhang, Y.; Tao, S., Global atmospheric emission inventory of polycyclic aromatic hydrocarbons (PAHs) for 2004. *Atmospheric Environment* **2009,** *43* (4), 812-819.
62. Harner, T.; Bidleman, T. F., Octanol−Air Partition Coefficient for Describing Particle/Gas Partitioning of Aromatic Compounds in Urban Air. *Environmental Science & Technology* **1998,** *32* (10), 1494-1502.
63. Jia, C.; Batterman, S., A Critical Review of Naphthalene Sources and Exposures Relevant to Indoor and Outdoor Air. *International Journal of Environmental Research and Public Health* **2010,** *7* (7), 2903-2939.
64. Li, G.; Xia, X.; Yang, Z.; Wang, R.; Voulvoulis, N., Distribution and sources of polycyclic aromatic hydrocarbons in the middle and lower reaches of the Yellow River, China. *Environmental Pollution* **2006,** *144* (3), 985-993.
65. Doong, R.-a.; Lin, Y.-t., Characterization and distribution of polycyclic aromatic hydrocarbon contaminations in surface sediment and water from Gao-ping River, Taiwan. *Water research* **2004,** *38* (7), 1733-1744.
66. Tao, Y.; Yu, J.; Lei, G.; Xue, B.; Zhang, F.; Yao, S., Indirect influence of eutrophication on air–water exchange fluxes, sinking fluxes, and occurrence of polycyclic aromatic hydrocarbons. *Water Research* **2017,** *122*, 512-525.
67. Friedman, C. L.; Zhang, Y.; Selin, N. E., Climate change and emissions impacts on atmospheric PAH transport to the Arctic. *Environmental Science & Technology* **2014,** *48* (1), 429-437.
68. Jesus, F.; Pereira, J. L.; Campos, I.; Santos, M.; Ré, A.; Keizer, J.; Nogueira, A.; Gonçalves, F. J. M.; Abrantes, N.; Serpa, D., A review on polycyclic aromatic hydrocarbons distribution in freshwater ecosystems and their toxicity to benthic fauna. *Science of The Total Environment* **2022,** *820*, 153282.
69. Guan, Y.-F.; Sun, J.-L.; Ni, H.-G.; Guo, J.-Y., Sedimentary record of polycyclic aromatic hydrocarbons in a sediment core from a maar lake, Northeast China: evidence in historical atmospheric deposition. *Journal of Environmental Monitoring* **2012,** *14* (9), 2475-2481.
70. Li, P.; Xue, R.; Wang, Y.; Zhang, R.; Zhang, G., Influence of anthropogenic activities on PAHs in sediments in a significant gulf of low-latitude developing regions, the Beibu Gulf, South China Sea: distribution, sources, inventory and probability risk. *Marine Pollution Bulletin* **2015,** *90* (1-2), 218-226.
71. Liu, G.; Zhang, G.; Jin, Z.; Li, J., Sedimentary record of hydrophobic organic compounds in relation to regional economic development: a study of Taihu Lake, East China. *Environmental Pollution* **2009,** *157* (11), 2994-3000.
72. Tang, Z.; Guo, J.; Liao, H.; Zhao, X.; Wu, F.; Zhu, Y.; Zhang, L.; Giesy, J. P., Spatial and temporal distribution and sources of polycyclic aromatic hydrocarbons in sediments of Taihu Lake, eastern China. *Environmental Science and Pollution Research* **2015,** *22* (7), 5350-5358.

73. Dat, N.-D.; Chang, M. B., Review on characteristics of PAHs in atmosphere, anthropogenic sources and control technologies. *Science of The Total Environment* **2017,** *609*, 682-693.
74. Abdel-Shafy, H. I.; Mansour, M. S., A review on polycyclic aromatic hydrocarbons: source, environmental impact, effect on human health and remediation. *Egyptian Journal of Petroleum* **2016,** *25* (1), 107-123.
75. Li, R.; Hua, P.; Cai, J.; Wang, X.; Zhu, Y.; Huang, Z.; Li, P.; Wang, Z.; Bai, Y.; Hu, B. X., A sixteen-year reduction in the concentrations of aquatic PAHs corresponding to source shifts in the Elbe River, Germany. *Journal of Cleaner Production* **2019,** *223*, 631-640.
76. Lou, S.; Shrivastava, M.; Ding, A.; Easter, R. C.; Fast, J. D.; Rasch, P. J.; Shen, H.; Massey Simonich, S. L.; Smith, S. J.; Tao, S.; Zelenyuk, A., Shift in Peaks of PAH-Associated Health Risks From East Asia to South Asia and Africa in the Future. *Earth's Future* **2023,** *11* (6), e2022EF003185.
77. Aben, R. C. H.; Barros, N.; van Donk, E.; Frenken, T.; Hilt, S.; Kazanjian, G.; Lamers, L. P. M.; Peeters, E. T. H. M.; Roelofs, J. G. M.; Domis, L. N. d. S.; Stephan, S.; Velthuis, M.; Van de Waal, D. B.; Wik, M.; Thornton, B. F.; Wilkinson, J.; DelSontro, T.; Kosten, S., Cross continental increase in methane ebullition under climate change. *Nature Communications* **2017,** *8*.
78. Nam, K. J.; Li, Q.; Heo, S. K.; Tariq, S.; Loy-Benitez, J.; Woo, T. Y.; Yoo, C. K., Inter-regional multimedia fate analysis of PAHs and potential risk assessment by integrating deep learning and climate change scenarios. *Journal of Hazardous Materials* **2021,** *411*, 125149.
79. Zhang, J.-Q.; Hu, T.-P.; Xing, X.-L.; Zheng, H.; Zhang, L.; Zhan, C.-L.; Liu, H.-X.; Xiao, W.-S.; Qi, S.-H., Distribution, sources and risk assessment of the PAHs in the surface sediments and water from the Daye Lake. *Huan Jing Ke Xue* **2017,** *38* (1), 170-179.
80. Yin, K.; Viana, P. Z.; Rockne, K. J., Organic contaminated sediments remediation with active caps: Nonlinear adsorption unveiled by combined isotherm and column transportation studies. *Chemosphere* **2019,** *214*, 710-718.
81. Li, F.; Chen, J.; Hu, X.; He, F.; Bean, E.; Tsang, D. C. W.; Ok, Y. S.; Gao, B., Applications of carbonaceous adsorbents in the remediation of polycyclic aromatic hydrocarbon-contaminated sediments: A review. *Journal of Cleaner Production* **2020,** *255*, 120263.
82. Hao, Z.; Wang, Q.; Yan, Z.; Jiang, H., Novel magnetic loofah sponge biochar enhancing microbial responses for the remediation of polycyclic aromatic hydrocarbons-contaminated sediment. *Journal of Hazardous Materials* **2021,** *401*, 123859.
83. Kumar, M.; Bolan, N. S.; Hoang, S. A.; Sawarkar, A. D.; Jasemizad, T.; Gao, B.; Keerthanan, S.; Padhye, L. P.; Singh, L.; Kumar, S.; Vithanage, M.; Li, Y.; Zhang, M.; Kirkham, M. B.; Vinu, A.; Rinklebe, J., Remediation of soils and sediments polluted with polycyclic aromatic hydrocarbons: To immobilize, mobilize, or degrade? *Journal of Hazardous Materials* **2021,** *420*, 126534.